Proceedings of the ASME 2018 International Mechanical Engineering Conference and Exposition
IMECE2018
November 9-15, 2018, Pittsburgh, PA, USA

IMECE2018-87521

THE VALUE OF ENERGY FLEXIBILITY: INTEGRATING WIND RESOURCES IN NEW YORK STATE

Terence M. Conlon*
Sustainable Engineering Laboratory
Dept. of Mechanical Engineering
Columbia University
New York, New York 10027
Email: tmc2180@columbia.edu

Vijay Modi
Sustainable Engineering Laboratory
Dept. of Mechanical Engineering
Columbia University
New York, New York 10027
Email: modi@columbia.edu

Michael B. Waite
Sustainable Engineering Laboratory
Dept. of Mechanical Engineering
Columbia University
New York, New York 10027
Email: mbw2113@columbia.edu

ABSTRACT

This paper explores the effects of energy system flexibility on the contribution of wind generation to the New York State (NYS) electricity generation mix. First, the benefits of NYS-specific flexible hydropower are investigated. For all simulations, a mixed integer linear program minimizes net load to determine the maximum aggregate capacity factor for the installed wind power. A similar routine explores the benefits of three different types of energy flexibility: flexible supply, flexible demand, and bidirectional flexibility (i.e. energy storage). To compare across technologies, a novel method of standardizing flexibility inputs, Potential Flexible Energy (PFE), is introduced.

With 30 GW wind capacity in NYS (average electricity demand of 18.7 GW), introducing electric vehicles with an average load of 1.44 GW and daily available battery capacity of 34.5 GWh (roughly equivalent to the daily use of 3.4 million passenger EVs) increases statewide wind utilization by 840 MW (9.0% of wind potential and 4.5% of average load). Added flexibility in the form of energy storage yields similar results: with 3.2 GW charge/discharge capability and 76.8 GWh storage capacity, statewide wind utilization increases by an average of 660 MW (7.0% of wind potential and 3.5% of average load).

Because of transmission constraints and the geographic distribution of high-potential wind resources, increased wind utilization is only achieved when flexibility is added in the region where 86% of the 30 GW simulated wind capacity is located.

1 INTRODUCTION

The use of renewable energy technologies to decrease fossil fuel emissions and mitigate the effects of climate change are well known [1, 2]. Driven by decreasing costs and growing societal awareness of the hazards of burning carbon fuels, solar and wind power penetration will increase throughout next century, as will the challenges of integrating these inflexible, low carbon resources [3, 4]. Among energy system planners, there is much debate over how to meet these challenges, which arise from the intermittent and stochastic nature of wind and solar generation [5–7]. The technologies and methods under discussion enable renewable energy integration in various ways, and include: carbon pricing; a well dispersed portfolio of energy sources; advanced grid monitoring and communication; expanded transmission capabilities; interconnection between regional systems; and increased system flexibility [8–12]. Previous research has focused on the benefits and challenges of deep penetration of Variable Renewable Energy (VRE) resources in New York State by significantly increasing the modeled capacity of wind and solar installations [13,14]. This paper will investigate the effects of expanded wind capacities with varied amounts of complementary flexibility. Here, flexibility is defined as "the extent to which a power system can modify its electricity production and consumption in response to variability, expected or otherwise" [15]. First, this paper explores the potential of hydropower to offer system flexibility and to increase consumption of wind generated energy, as flexible use of hydroelectric resources offers clear benefits to

*Address all correspondence to this author.

Nomenclature

Variables

B	baseload electricity generation (MW)
CF	capacity factor
D	electrical demand (MW)
E	reservoir energy level (MW)
H	hydropower generation (MW)
G	curtailment (MW)
I	import from external interface (MW)
L^+	positive flow transmission limit (MW)
L^-	negative flow transmission limit (MW)
l	transmission line loss factor
NL	net load (MW)
N	nuclear generation (MW)
n_r	set of sites in a region
PS	pumped storage generation (MW)
R	set of all regions
S	solar generation (MW)
T	total number of hourly time steps
U	wind generated energy used (MW)
W	potential wind output (MW)
x_h	fraction flexible hydropower
Z	transmission (MW)
η	generating/charging efficiency
τ	time constant

Subscripts

bg	Blenheim-Gilboa
$elec$	electric
ev	electric vehicle
fh	flexible hydro
fix	fixed
$flex$	flexible
h	hydroelectric
in	inflow
lew	Lewiston
nc	new pumped storage capacity
nia	Niagara
$nyiso$	NYISO-reported
ps	pumped storage
r	region
r'	adjacent region
s	site
sh	small hydro
stl	St. Lawrence

Abbreviations

CFM	comparative flexibility model
FHM	flexible hydropower model
$MILP$	mixed integer linear program
$PHES$	pumped hydro energy storage
VRE	variable renewable energy

power systems [16–18]. The authors conducted a comprehensive review of the state's hydropower resources in order to create a mixed-integer linear program (MILP), the *Flexible Hydropower Model* (FHM), which optimizes NYS system response to up to 30 GW of wind capacity by minimizing net load. The simulated hydropower flexibility reflects current load-following capabilities of NYS hydro resources. To accurately assess the benefits of hydropower flexibility, solutions from the MILP are compared to a baseline case in which the state's hydroelectric generation is the result of smoothing reported generation values over two weeks. Expanding the scope of study, this paper next evaluates the impact of three different types of power system flexibility: supply-side flexibility, demand-side flexibility, and bidirectional flexibility. A similar MILP, the *Comparative Flexibility Model* (CFM), was created to complete this analysis, where results are again compared to a baseline case with fixed generation.

The structure of the paper is as follows: Section 2 presents background information on hydropower resources in NYS. Section 3 details the FHM and CFM methodologies and the data inputs used to parameterize and run the models. Section 4 discusses the FHM and CFM results. Section 5 restates the paper's most salient conclusions and offers directions for future work.

2 BACKGROUND

2.1 NYS Hydropower Resources

In New York State, four hydroelectric power plants constitute 80% of the state's total hydropower capacity and 83.2% of all hydro generation, providing 13.3% of all statewide electricity generation. The largest of these generation facilities is the Robert Moses Niagara Hydroelectric Power Station. The Moses-Niagara plant has a rated capacity of 2460 MW, and in 2016, generated 54% of the state's hydropower [19]. In accordance with the 1950 Niagara Treaty between the United States and Canada, a portion of the Niagara River is diverted into the Moses-Niagara forebay after allowing for the necessary flow of water over Niagara Falls and into the Sir Adam Beck Hydroelectric Generation Facility, a hydro-plant on the Canadian side of the river [20].

The Moses-Niagara forebay also serves as the lower reservoir of the Lewiston Pumped Hydro Energy Storage (PHES) plant. During periods of low statewide electricity consumption, the Lewiston Plant pumps water from the Moses-Niagara forebay into its upper reservoir. During periods of high statewide demand, the Lewiston Plant generates electricity by allowing water to flow from its upper reservoir back into the Moses-Niagara forebay. The generating capacity of Lewiston is 240 MW. In 2016, the Lewiston plant generated 1.7% of NYS hydropower [19].

The Moses-Saunders Power Dam provides the second most hydropower to the state. The dam straddles the St. Lawrence River and diverts water to two adjacent power stations, the American St. Lawrence-Franklin D. Roosevelt Power Project and the

Canadian R.H. Saunders Generating Station. Both facilities operate as run-of-the-river plants with limited storage capability. The St. Lawrence-FDR facility has a total rated power capacity of 912 MW. Because of reliable flow, St. Lawrence-FDR operates near its maximum generation capacity nearly all year long. In 2016, St. Lawrence-FDR generated 26.0% of NYS hydropower [19].

The last of the four large hydroelectric power plants is the Blenheim-Gilboa PHES facility, which has the second largest total rated turbine capacity in the state at 1160 MW [21]. Its upper reservoir has a capacity of 18 million cubic meters, which corresponds to approximately 14 hours of peak generating capability. In effect, Blenheim-Gilboa operates as a closed system with 73% efficiency, as the Schoharie Creek water replenishes water lost or evaporated. The Blenheim-Gilboa plant supplies the New York Independent System Operator (NYISO) with black-start capability; in 2016, it supplied 1.4% of NYS hydropower [19].

Smaller hydropower facilities constitute the remaining 20% of hydroelectric resources in New York, supplying 16.8% of the state's hydroelectric power [19]. Throughout this paper, these plants are lumped together to yield one representative facility, subsequently referred to as 'Small Hydro', with a rated power capacity of 1230 MW.

2.2 Moses-Niagara Energy Inflow

This study computed energy inflow to the Moses-Niagara forebay based on flow measurements of the Niagara River [24] and the specifics of the 1950 Niagara Treaty between the US and Canada [20]. The Niagara Treaty establishes that 100,000 cubic feet per second of water must pass over Niagara Falls, downstream of the hydropower facility intakes, between the hours of 8am and 10pm EST from April 1st to September 15th, inclusive; and each day between 8am and 8pm EST from September 16th to October 31st, inclusive. The flow over the falls should never drop below 50,000 cubic feet per second at any other time. On the American side, the drawing capacity of the Moses-Niagara plant is limited to 109,000 cubic feet per second by the size of the canal that diverts water from the Niagara River to the forebay.

After applying these constraints to the river flow readings, the authors determined the time series for water inflow to the Niagara-Moses facility. With assumed turbine efficiency of 0.90, generator efficiency of 0.96, and a 91.44 meter head, the yearly energy inflow to Moses-Niagara was calculated to be 14.409 TWh in 2016, nearly equal to the EIA-reported energy generation of 14.410 TWh that year [19]. As such, the authors feel justified using this method to determine the Niagara-Moses energy inflow time series.

2.3 St. Lawrence-FDR Energy Inflow

The Ontario ISO, IESO, publishes hourly generation and generation capacity data for every plant larger than 20 MW in the region [25]. Because of the twin nature of the St. Lawrence-FDR and the R.H. Saunders hydroelectric facilities — both facilities are supplied by the Moses-Saunders Power Dam and are therefore subject to the same water inflows and weather conditions — the authors assumed that the IESO-reported hourly generation capacity for 2016 applied similarly to the St. Lawrence-FDR plant after scaling for differences in rated power capacity (912 MW for St. Lawrence-FDR and 1045 MW for R.H. Saunders). On account of the St. Lawrence-FDR facility's operation as a run-of-the-river hydroelectric plant, no storage capacity was assumed to exist. With a generator efficiency of 0.96, the yearly energy inflow to St. Lawrence-FDR was calculated to be 7.05 TWh in 2016, slightly less than the EIA-reported generation of 7.10 TWh that year.

2.4 Small Hydro Energy Inflow and Storage

The energy inflow to the representative Small Hydro facility, $H^t_{in,sh}$, was determined by smoothing the difference of the NYISO-reported hydropower generation (H^i_{nyiso}) and the calculated energy inflow to both the Moses-Niagara ($H^i_{in,nia}$) and St. Lawrence-FDR ($H^i_{in,stl}$) generation facilities with a smoothing factor τ = 336 hours (2 weeks):

$$H^t_{in,sh} = \frac{1}{\tau+1} \sum_{i=t-\tau/2}^{t+\tau/2} H^i_{nyiso} - H^i_{in,nia} - H^i_{in,stl} \qquad (1)$$

The authors believe the approximation justified: the large generation facilities not accounted for in this equation (Lewiston, Blenheim-Gilboa) are pumped storage plants and accordingly have no significant energy influxes. Therefore, all other hydro inflows must be captured by the remaining Small Hydro plant. To ensure that the Small Hydro inflow is not a direct response to the Moses-Niagara and St. Lawrence-FDR inflows, a smoothing factor τ-value of 2 weeks was used to smooth the difference of the hydro production and hydro inflows without allowing for the possibility of long-term storage. Smoothing the difference between hydropower production and known inflows ensures that the scale of the Small Hydro energy inflow is appropriate. Such an approach also ensures that $H^t_{in,sh}$ responds to macro-trends in water availability but not to small fluctuations in the flow of disconnected rivers.

For the Small Hydro representative facility, the energy from 24 hours of maximum generation was assumed as storage capacity.

2.5 No Flexibility Baseline

To compare the results of flexible hydropower operation, the authors analyzed a baseline, fixed hydropower simulation. For this control scenario, fixed hydropower generation at time t, H^t_{fix}, was set equal to the amount of hydropower reported by NYISO for that time step, H^i_{nyiso}, smoothed over τ = 336 hours:

$$H^t_{fix} = \frac{1}{\tau+1} \sum_{i=t-\tau/2}^{t+\tau/2} H^i_{nyiso} \tag{2}$$

3 METHODOLOGY

3.1 Flexible Hydropower Model Overview

The Flexible Hydropower Model uses the parameters of NYS hydropower facilities described in Section 2 to produce a MILP that minimizes net load in New York given capacities of installed wind generation and available PHES. Minimizing the sum of statewide net load achieves the highest degree of wind energy utilization for the assumed set of constraints. The MILP is solved at an hourly time resolution and ignores interzonal transmission constraints. The objective function for the FHM is presented below:

$$minimize \qquad \sum_{t \in T} NL^t \tag{3}$$

where,

$$NL^t = D^t_{nyiso} - (P^t_{nia} + P^t_{lew} + P^t_{bg} + P^t_{sh} + P^t_{nc}) - U^t - B^t \tag{4}$$

Here, the net load, NL^t, is defined by the exogenously determined statewide electricity demand, D^t_{nyiso}; and baseload renewable generation, B^t, where B^t is set equal to the sum of (1) nuclear generation, N^t; (2) solar generation, S^t; and (3) generation at the St. Lawrence-FDR facility, $H^t_{in,stl}$. It is also defined by the following state variables: generation at Moses-Niagara, P^t_{nia}; generation at Lewiston, P^t_{lew}; generation at Blenheim-Gilboa, P^t_{bg}; generation from the Small Hydro facility, P^t_{sh}; generation from any new, simulated PHES, P^t_{nc}; and utilized wind energy, U^t. A full list of constraints can be found in Appendix B. The model is formulated in MATLAB [26] and solved in Gurobi, a commercial optimization solver. [27].

Beginning December 2015, NYISO has published fuel mix data for the NYS electricity grid at 5-minute intervals [28]. The fuel mix data present the amount of total power supplied by generators classified as: nuclear, hydro, natural gas, dual fuel, wind, other renewables, and other fossil fuels. Five minute reported hydro data for 2016 — along with Niagara River streamflow and St. Lawrence rated generation capacities — were used to determine the Small Hydro energy inflow. After parameterizing the state's hydro resources, the authors used 6 years of NYISO-reported hourly demand data (2007-2012) to run the FHM. Nuclear generation in the state was taken as a constant 3026 MW, based on the annual nuclear energy reported by NYISO after removing the contribution from Indian Point Energy Center, as this plant is slated to be decommissioned as soon as 2021.

For some scenarios, the FHM simulated additional PHES in NYS. This additional storage was scaled in reference to the Blenheim-Gilboa facility: a scenario denoted "Flex Hydro + 3 PS" indicates statewide flexible hydro generation with additional PHES three times the size of Blenheim-Gilboa in both generation and reservoir capacity. Energy generated by this simulated plant, P^t_{nc}, allows the FHM to interrogate the benefits to an energy system when supplementary flexibility is present.

To simulate capacities of wind power far exceeding current levels, the FHM relied on model wind power data for 126,000 potential wind sites developed by the National Renewable Energy Laboratory (NREL) [32, 33]. A previous study found the NREL model to significantly overpredict the electricity generated at actual sites in NYS and developed a procedure to adjust the time series to reflect actual output [13]. For the current study, the authors employed the modified wind generation time series from this earlier study. In simulating increased wind power capacity, it was assumed that wind turbines are first installed at locations with the highest potential electricity generation, with additional turbines installed at progressively less productive sites.

In order to determine solar potential in NYS, the authors accessed the NYSERDA Distributed Generation Integrated Data System [23]. This resource reports the hourly generation time series of solar facilities in New York. With the rated capacities of these facilities, the hourly solar generation potential was calculated for the 10 largest plants in New York State that were operational for the entirety of 2016. These time series were averaged to yield the generation potential of a representative plant, which was then scaled by the installed solar capacity. It was assumed that 600 MW of solar capacity existed in NYS when running the FHM.

3.2 Comparative Flexibility Model Overview

The CFM also utilizes a MILP to minimize the sum of statewide net load given the presence of varying levels of VRE capacity and system flexibility. The objective function for the CFM is given as:

$$minimize \qquad \sum_{t \in T} \sum_{r \in R} NL^t_r \tag{5}$$

where,

$$NL_r^t = D_{elec,r}^t + D_{flex,r}^t - H_{flex,r}^t - PS_{gen,r}^t + PS_{pump,r}^t - U_r^t - B_r^t + \sum_{r' \in R} [Z_{rr'}{}^t - (1 - l_r) Z_{r'r}{}^t] \quad (6)$$

For every region r, at each time step t, the net load NL_r^t is partly defined by two exogenous variables: electricity demand, $D_{nyiso,r}^t$; and baseload renewable generation, B_r^t, where B_r^t is set equal to the sum of (1) nuclear generation, N_r^t; (2) solar generation, S_r^t; and (3) fixed hydropower generation, $H_{fix,r}^t$. The following state variables are also used: flexible demand, $D_{flex,r}^t$; generation from flexible hydropower, $H_{flex,r}^t$; pumped storage generation, $PS_{gen,r}^t$; pumped storage pumping, $PS_{pump,r}^t$; utilized wind energy, U^t; and net imports from adjacent regions after accounting for transmission losses, $\sum_{r' \in R} [Z_{rr'}{}^t - (1 - l_r) Z_{r'r}{}^t]$. A list of model constraints can be found in Appendix B. By minimizing the sum of the statewide net load, the CFM minimizes the amount of electricity generated by fossil fuel-based sources. The CFM is also formulated in MATLAB [26] and solved using Gurobi [27].

To simulate the spatial characteristics of load and generation in New York, this paper condenses the 11 NYISO load zones (A-K) into four regions (1-4) with interregional transmission limits equivalent to those given in [29]. The boundaries of these regions align with the main NYISO transmission system interfaces. Figure 1 shows the 11 NYISO load zones; the load zones, wind capacity (in the 30 GW wind scenario), and average electricity demand of each region are presented in Table 1. Transmission losses are assumed to be 3% between adjacent regions, ensuring that wind electricity is first used to meet demand nearest the region in which it was generated.

In the CFM, nuclear generation in the state was taken as a constant 3026 MW (all in Region 1), and solar and wind generation were calculated as described for the FHM (150 MW solar in each region). The daily hydro output was estimated based on the actual 2007-2012 monthly output for facilities in each zone [28] and a cubic spline function constrained to be continuous and smooth from month to month. In the flexible scenarios, a fraction (x_h) of the total hydro generation ($H_{tot,r}$) was assumed flexible, able to be dispatched with a degree of control; the balance of the hydro generation was simulated as non-flexible and needed to be consumed during the time-step it became available.

3.3 Modes of Flexibility

In the Comparative Flexibility Model, the authors analyzed three different modes of flexibility. The first is supply-side flexibility, of which a traditional hydroelectric plant is an example. Such a facility maintains a degree of control over when it generates electricity based on its ability to store water in its reservoir.

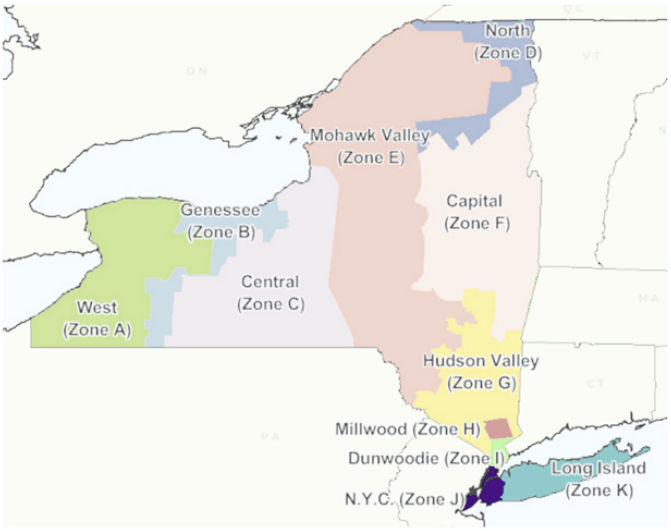

FIGURE 1: NYISO control area load zones [30].

TABLE 1: Spatial grouping of NYISO load zones; Distribution of wind capacity in 30 GW scenario [13]; Average 2007 – 2012 electricity demand [28].

Region	NYISO Zones	Wind Cap. (30 GW)	Avg. Demand
1	A, B, C, D, E	25814 MW	6382 MW
2	F, G	3358 MW	2495 MW
3	H, I, J	16 MW	7211 MW
4	K	812 MW	2567 MW

The second is demand-side flexibility (e.g. a fleet of electric vehicles with some discretion over when it can charge); this type of flexibility offers a degree of control over when certain electric loads can be met. The third type of flexibility is bidirectional energy storage; a plant with bidirectional flexibility can both absorb and deliver power, and thus has one greater degree of control than either flexible supply or flexible demand facilities.

3.4 Potential Flexible Energy

In order to compare the effects of the three types of flexibility, this paper proposes a metric, *Potential Flexible Energy (PFE)*. PFE is defined as *the potential amount of energy a flexible resource can generate or absorb over a period of time*. By equating PFE in all three flexibility cases, the authors ensure that no mode of flexibility allows the system to utilize more flexible energy over the analyzed time period. Because the analysis is per-

formed hourly over 6 years ($T = 52608$) and the different modes of flexibility operate on different time-scales, PFE is presented as an average hourly quantity. This has the units MWh/h; for simplicity, the authors use units MW. In this analysis, PFE is calculated before efficiency losses ($\eta_{gen}, \eta_{pump} = 0.894$; $\eta_{ev} = 0.95$).

PFE is determined in the following ways for the three modes of flexibility:

1. For flexible supply (traditional hydropower), PFE is equated to the average amount of energy that flows into the reservoir, H_{in}, over the analyzed time period:

$$PFE_{fh} = \frac{1}{T}\sum_{t}^{T} H_{in} \tag{7}$$

   The power of the supply-side facility is determined by dividing the average inflow power by an assumed capacity factor (CF) equal to 0.45; the reservoir is sized to hold 24 hours of max generation.

2. For flexible demand (electric vehicles), PFE is equated to the constant hourly EV load, D_{ev}:

$$PFE_{ev} = D_{ev} \tag{8}$$

   It is assumed that the daily EV load – $24 * D_{ev}$ – can be met anytime between 7pm and 7am. The power absorption capacity (i.e. maximum rate of charge) for the EVs is set to $6 * D_{ev}$.

3. For energy storage (i.e. PHES), PFE is computed from the facility's generation capacity and a maximum capacity factor:

$$PFE_{ps} = CF_{max} * P_{gen,ps} \tag{9}$$

   If we were to ignore charging and discharging efficiencies, the maximum possible capacity factor would be 0.5, since all energy provided in discharge must be stored by charging; however, we take into account these efficiencies and arrive at $CF_{max} = 0.45$. The energy storage capacity of the resource is 24 hours of peak discharge capability. Therefore, with $CF_{max} = 0.45$, the energy storage capacity and discharge capability equal those of the traditional hydropower model for a given quantity of PFE.

For $PFE = 1440MW$, the power and energy characteristics for the three different types of flexibility are given in Table 2. This quantity represents approximately one-half the average statewide hydropower production over the six-year time horizon (2.99 GW), and in the opinion of the authors, offers a degree of flexibility reasonable for an energy system the size of New York State's.

TABLE 2: Generation/absorption and energy storage capacities for different flexibility types for 1440 MW PFE.

Flex. Type	Gen./Abs. Cap.	Energy Storage Cap.
Flex. Supply	3.2 GW	76.8 GWh
PHES	3.2 GW	76.8 GWh
EV Flex.	8.64 GW	34.56 GWh

4 RESULTS

4.1 Flexible Hydropower Model

Results from the FHM indicate that flexible hydropower allows for greater utilization of wind-generated electricity at deep penetrations; additional PHES capacity further increases utilization. Figure 2 presents the statewide energy mix with wind capacities of 10 GW and 30 GW, each for the following flexibility scenarios: no flexibility ("No Flex"), hydropower supply flexibility ("Flex Hydro"), and hydropower supply flexibility plus energy storage equivalent to three times the size of Blenheim-Gilboa ("Flex Hydro + 3PS").

With 10 GW wind capacity, the "Flex Hydro" and "Flex Hydro + 3PS" scenarios have minimal effect on the statewide energy mix (<0.5%); because curtailment is low at this wind capacity, flexibility measures have little impact. However, with 30 GW wind capacity, the simulated flexibility allows for a higher degree of wind power utilization. At this capacity, the "Flex Hydro + 3PS" scenario increases wind utilization by 1.2 GW (12.7% of potential wind generation and 6.4% of average load) compared to the scenario without flexibility.

4.2 Comparative Flexibility Model

In the CFM, we expand on the FHM by (a) investigating additional degrees of flexibility and (b) including the effects of interregional transmission limits. Five scenarios are considered:

1. No flexibility ("No Flex."),
2. Flexible hydropower supply ("Flex. Hydro"),
3. Energy storage simulated as PHES,
4. Demand flexibility simulated as electric vehicles ("EV Demand Flex."), and
5. A comparison to an equivalent system with no transmission limits ("No Trans. Lim.").

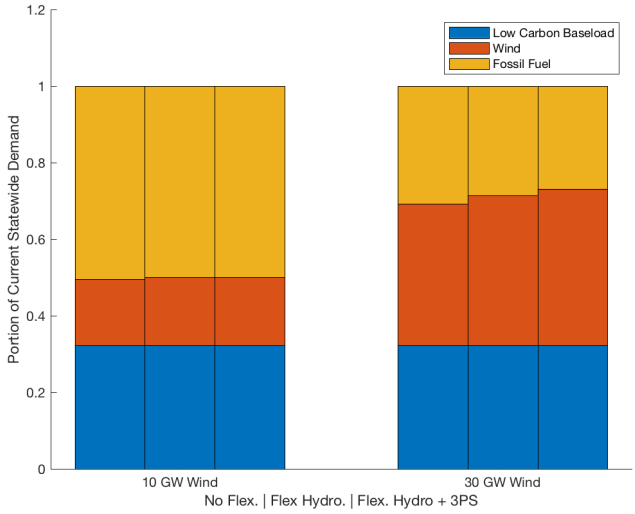

FIGURE 2: FHM-computed statewide energy mix for flexibility type for 10 GW and 30 GW wind scenarios; each grouping of columns corresponds to implementations of flexibility for the given wind capacity.

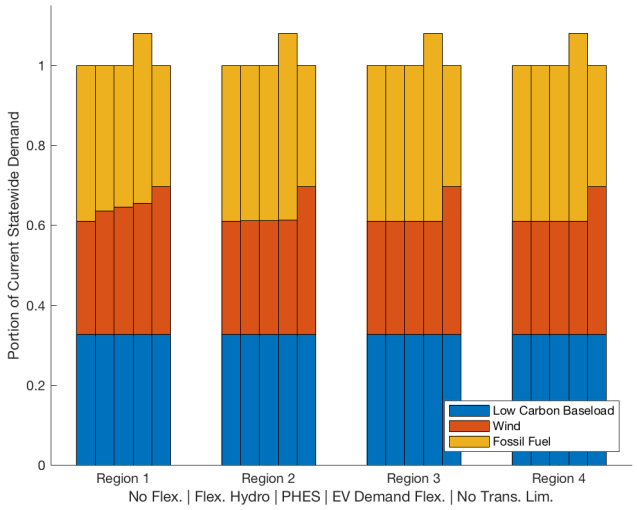

FIGURE 3: CFM-computed statewide energy mix for flexibility type by region; each grouping of columns corresponds to implementations of flexibility in the noted region; 30 GW of statewide wind capacity.

For each of these scenarios, the different types of flexibility are (a) simulated alone without other flexibility measures and (b) within single geographical areas corresponding to the Regions defined in Table 1. To clearly illustrate our findings, only the 30 GW statewide wind capacity scenario is presented and a single Potential Flexible Energy (PFE) amount of 1440 MW was used for all simulations. We retain the metric of computing the share of statewide electricity demand met by wind.

Flexibility in Region 1 has the largest effect on statewide consumption of wind energy, while flexibility in Region 2 has only marginal effects, and flexibility in Regions 3 and 4 has negligible impact on the amount of wind power utilized. Figure 3 — with columns grouped by region showing each of the five flexibility scenarios simulated in the indicated region — shows the share of statewide demand met by low carbon baseload generation (nuclear and hydropower) and wind power, with the balance assumed to be met by fossil fuel-based generation.

Without flexibility, wind-generated electricity contributes a computed average 5300 MW (28.4% of total electricity demand). Flexibility measures placed in Region 1 increase the contribution from wind by an average 470 MW (5.0% of potential wind generation and 2.5% of average load) with hydropower supply flexibility, an average 660 MW (7.0% of potential wind generation and 3.5% of average load) with PHES, and an average 840 MW (9.0% of potential wind generation and 4.5% of average load) with EV demand flexibility. It should be noted that the increase in wind-generated electricity utilization with EVs is a result of both additional demand and the flexibility of that demand: An average 720 MW increase in wind utilization is the result of the additional demand and an average 120 MW is due to its flexibility. Removing all transmission limits results in 37.0% of demand being met by wind, a result which is consistent with the FHM results in Figure 2.

As noted, flexibility in Regions 2, 3, and 4 has little effect on wind utilization. This outcome indicates that flexibility in New York's downstate regions would have little impact on reducing curtailment of wind-generated electricity — predominantly located at high-potential sites in Region 1 — due to the existing transmission limits. A wider implication beyond this specific case study is that VRE integration measures in a transmission-constrained energy system are likely to have the most impact if located near the VRE resource. By investigating a few select scenarios in detail, the overall effects described above become clearer. Figure 4 shows the regional contribution of low carbon baseload generation, wind, and fossil fuels for three scenarios compared to the no-flexibility baseline: (a) energy storage, PHES, in Region 1; (b) demand flexibility, EVs, in Region 1; and (c) demand flexibility, EVs, in Region 2.

Outlining the results of the no-flexibility scenario defines the general topology of energy utilization in the system: Region 1, which contains 86% of the state's 30 GW wind power capacity, 91% of the state's hydropower generation, and 100% of the state's simulated nuclear generation, meets nearly its entire electricity load with low-carbon energy. Region 2, which benefits

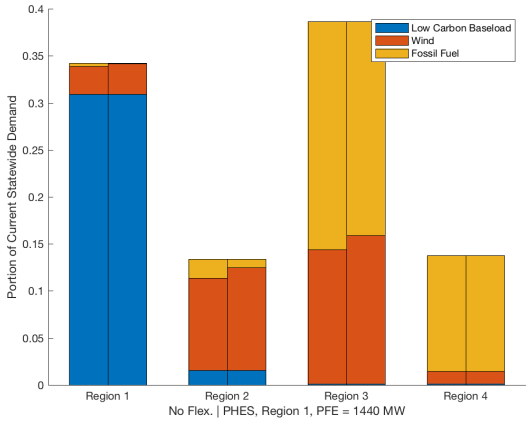

(a) No Flex. | PHES, Region 1

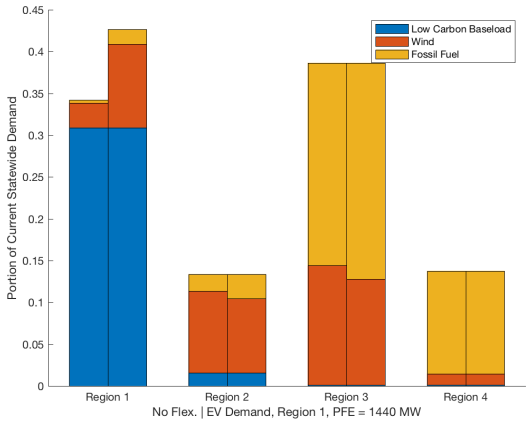

(b) No Flex. | EV Demand Flex., Region 1

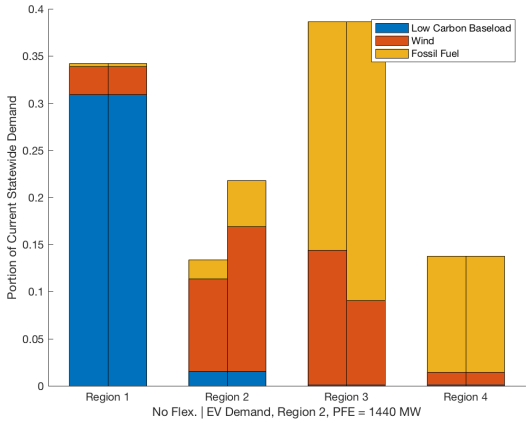

(c) No Flex. | EV Demand Flex., Region 2

FIGURE 4: Regional energy mixes for 3 different flexibility scenarios, normalized by state load. Each breakdown is juxtaposed with the energy mix breakdown from the no flexibility scenario.

from its proximity to Region 1, meets a majority of its statewide demand from wind energy generated in the two regions. Region 3, which includes much of the New York City metropolitan area, has no low-carbon baseload energy generation within its boundaries; in the 30 GW wind power scenario, a significant portion of Region 3's load is met by wind generation from the west, but more than half of the region's demand is provided by fossil fuel generators. Region 4, at the grid "edge" and distant from wind-rich regions, has the highest portion of load met by high-carbon sources.

Figure 4(a) compares the computed regional energy mix for the "PHES, Region 1" scenario to that of the no flexibility scenario. As PHES increases the wind energy utilized overall, increases in demand met by wind are computed for Regions 1-3 with no effect on Region 4. This suggests that storage is effective at retaining the electricity generated by wind for discharge to other regions when transmission capacity becomes available.

Figure 4(b) shows that with EV demand flexibility in Region 1, the increase in electricity demand (and the flexibility of that demand) allows for significantly more wind to be used to meet loads in that region. However, some decrease in wind-generated electricity used to meet loads in Regions 2 and 3 results from this electricity being used nearer the wind resource in Region 1. On balance, as is shown in Figure 3, EVs in this region significantly increase overall wind utilization.

Figure 4(c) shows that increased EV demand in Region 2 results in (a) an increase in wind utilization in Region 2, and (b) a similarly sized reduction in wind utilization in Region 3. Therefore, increased wind utilization in Region 2 displaces wind utilization in Region 3. The aggregate effect is a negligible increase in overall wind utilization shown in Figure 3, above.

The inference related to the transmission effects on the results shown in Figure 4(a) is further supported by computing the loading of interregional transmission interfaces. Figure 5 shows the amount of electricity transmitted at the interregional interfaces with and without PHES in Region 1. With an uptick in wind-generated electricity utilization in Regions 2 and 3, increased utilization of transmission capacity at Region 1-2 and Region 2-3 interfaces are also computed; the Region 3-4 interface displays no such effect. Without flexibility, the Region 1-2 transmission capacity is full more than half the simulation time period. Some increase in times of full loading is computed with PHES; however, most of the increased energy flow (entirely constituted of additional wind-generated electricity) occurs at times of lower transmission loading, supporting our earlier conclusion.

5 CONCLUSION

This paper presents two models, both of which seek to quantify the benefits of power system flexibility to New York State under different considerations. The Flexible Hydropower Model (FHM) investigates different levels of hydropower flexi-

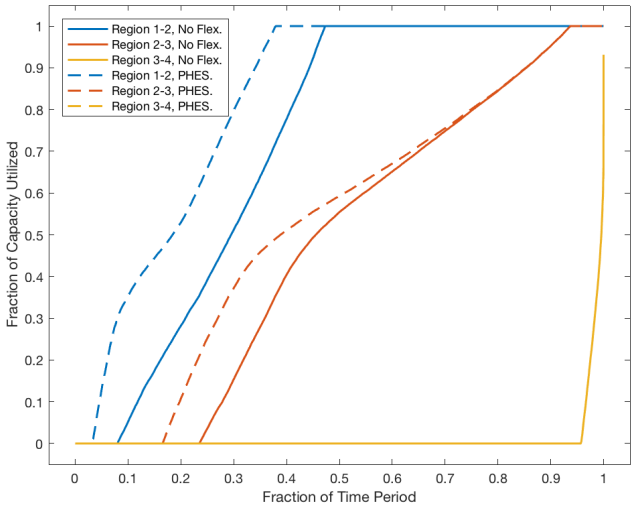

FIGURE 5: Normalized transmission loading duration curve vs. time; PHES in Region 1, PFE = 1440 MW.

bility compared to a fixed hydropower baseline to simulate the state's current load-following hydropower capability in the context of deep VRE penetration. Simulated flexibility offers system benefits only at installed wind capacities above 10 GW; at 30 GW wind capacity, flexible hydropower with additional PHES increases average wind utilization by 1.2 GW (12.7% of wind potential and 6.4% of average load).

The Comparative Flexibility Model (CFM) explores different types of system flexibility. Results show that energy storage (in the form of PHES) and demand-side flexibility (in the form of electric vehicles) have the largest effect on integrating substantial capacities of renewable generation when located near the VRE resource. The adoption of electric vehicles in Region 1 with an average load of 1.44 GW and daily available battery capacity of 34.5 GWh increases average statewide wind utilization by 840 MW (9.0% of potential wind generation and 4.5% of average load) in a 30 GW wind capacity scenario; PHES in Region 1 with 3.2 GW charge/discharge capability and 76.8 GWh storage capacity expands statewide wind utilization by an average of 660 MW (7.0% of wind potential and 3.5% of average load).

A central finding of this study is that in the transmission-constrained system simulated, flexibility only increases wind-generated electricity utilization when located near the wind resource, which is primarily in Region 1. All types of flexibility in Region 2-4 have negligible impact on increasing wind-generated electricity utilization. Therefore, energy systems planners should prioritize siting large-scale flexibility measures near the renewable generation.

Further research is needed to generalize the results of this paper for other VRE resources, namely solar photovoltaics and offshore wind power. Offshore wind power is often nearer transmission-constrained load centers that are distant from onshore wind resources. Tradeoffs between these effects and the costs and opportunities for expanded transmission capacity also require investigation.

ACKNOWLEDGMENT

Partial support for this research was provided by National Science Foundation Grant 1639214 [Innovations at the Nexus of Food, Energy, and Water Systems (Track 1): Understanding multi-scale resilience options for vulnerable regions].

REFERENCES

[1] International Energy Agency. (2017). Getting Wind and Sun onto the Grid A Manual for Policy Makers, 64.

[2] International Energy Agency. (2017). The Status of Power System Transformation.

[3] Cole, W., Frew, B., Mai, T., Bistline, J., Blanford, G., Young, D., Donohoo-Vallett, P. (2017). Variable Renewable Energy in Long-Term Planning Models : A Multi-Model Perspective Variable Renewable Energy in Long-term Planning Models. (November 2017), 35.

[4] Williams JH, Debenedictis A, Ghanadan R, Mahone A, Moore J, et al. (2012). 2050: The pivotal role of electricity. Science, 335:5360.

[5] Jacobson MZ, Delucchi MA, Cameron MA, Frew BA. Low-cost solution to the grid reliability problem with 100% penetration of intermittent wind, water, and solar for all purposes. Proc Natl Acad Sci USA, 2016.

[6] MacDonald A, Clack C, Alexander A, et al. Future cost-competitive electricity systems and their impact on US CO2 emissions. Nature Climate Change, 2016.

[7] Bistline, J. E., Blanford, G. J. (2016). More than one arrow in the quiver: Why 100% renewables misses the mark. Proceedings of the National Academy of Sciences, 113(28), E3988E3988.

[8] Kern J, Patino-Echeverri D, Characklis G. An integrated reservoir-power system model for evaluating the impacts of wind integration on hydropower resources. Renewable Energy, 2014.

[9] Cochran, J., Bird, L., Heeter, J., Arent, D. J. (2014). Integrating Variable Renewable Energy in Electric Power Markets: Best Practices from International Experience, (April).

[10] Bird, L., Lew, D., Milligan, M., Carlini, E. M., Estanqueiro, A., Flynn, D., Miller, J. (2016). Wind and solar energy curtailment: A review of international experience. Renewable and Sustainable Energy Reviews, 65, 577586.

[11] Gunther, S., Bensmann, A., & Hanke-Rauschenbach, R. (2018). Theoretical dimensioning and sizing limits of hybrid energy storage systems. Applied Energy, 210(October 2017), 127137.

[12] Auer H, Haas R. On integrating large shares of variable renewables into the electricity system. Energy, 2016.

[13] Waite M, Modi V. Modeling wind power curtailment with increased capacity in a regional electricity grid supplying a dense urban demand. Applied Energy, 2016.

[14] Jacobson, M. Z., Howarth, R. W., Delucchi, M. A., Scobie, S. R., Barth, J. M., Dvorak, M. J., Ingraffea, A. R. (2013). Examining the feasibility of converting New York States all-purpose energy infrastructure to one using wind, water, and sunlight. Energy Policy, 57, 585601.

[15] Olivella-Rosell, P., Bullich-Massague, E., Aragues-Penalba, M., ... Villafafile-Robles, R. Optimization problem for meeting distribution system operator requests in local flexibility markets with distributed energy resources. Applied Energy, Volume 210, 2018, Pages 881-895.

[16] Huertas-Hernando D, Farahmand H, Holtinnen H, et al. Hydro power flexibility for power systems with variable renewable energy sources: an IEA Task 225 collaboration. Wiley Interdisciplinary Reviews: Energy and Environment, 2017.

[17] Hirth L. The benefits of flexibility: The value of wind energy with hydropower. Applied Energy, 2016.

[18] Cutululis N, Farahmand H, Jaehnert S, et al. Hydropower flexibility and transmission expansion to support integration of offshore wind. Offshore Wind Farms: Technologies, Design, and Operation, 2016.

[19] US Energy Information Agency. Form EIA-860 detailed data. Accessed at *https://www.eia.gov/electricity/data/eia860/.*

[20] International Niagara Board of Control. Section 2: The 1950 Niagara Treaty. Accessed at: *www.ijc.org*

[21] New York Power Authority. Draft Application for New License for Major Project — Existing Dam. Blenheim-Gilboa Pumped Storage Power Project. Exhibit A. December 2016.

[22] New York Power Authority. Draft Application for New License for Major Project — Existing Dam. Blenheim-Gilboa Pumped Storage Power Project. Exhibit B. December 2016.

[23] New York State Energy Research and Development Authority. Distributed Generation Integrated Data System. Accessed at: *http://dg.nyserda.ny.gov/reports/.*

[24] Canadian Water Office. Real Time Hydrometric Data for NIAGARA RIVER AT FORT ERIE (02HA013) [ON]. Accessed at: *https://wateroffice.ec.gc.ca/report*

[25] The Independent Electricity System Operator. Accessed at: *http://www.ieso.ca/en/power-data/supply-overview/transmission-connected-generation*

[26] MATLAB and Statistics Toolbox Release 2012b, The MathWorks, Inc., Natick, Massachusetts, United States.

[27] Gurobi Optimization Inc., Gurobi Optimizer Version 7.0, (2016).

[28] The New York Independent System Operator. Data accessed at: *http://www.nyiso.com/public*

[29] New York Independent System Operator. 2016 Reliability Needs Assessment, Final Report. October 18, 2016.

[30] Image source: FERC. Accessed at: *http://www.rtoinsider.com/ferc-nyiso-icap-market-power-mitigation-14452/*

[31] The American Wind Energy Association. US Wind Energy State Facts. Accessed March 2018.

[32] Draxl, C., B.M. Hodge, A. Clifton, and J. McCaa. 2015. Overview and Meteorological Validation of the Wind Integration National Dataset Toolkit (Technical Report, NREL/TP-5000-61740). Golden, CO: National Renewable Energy Laboratory.

[33] Draxl, C., B.M. Hodge, A. Clifton, and J. McCaa. 2015. "The Wind Integration National Dataset (WIND) Toolkit."

Applied Energy 151: 355366.
[34] The Office of Highway Policy Information, the Federal Highway Administration. Highway Statistics Series, State Statistical Abstracts 2015. https://www.fhwa.dot.gov/policyinformation/statistics/abstracts/2015/state.cfm?loc=ny.
[35] Ueckerdt, Falko, Lion Hirth, Gunnar Luderer & Ottmar Edenhofer (2013): System LCOE: What are the costs of variable renewables?, Energy 63, 61-75.
[36] Luderer, G., Pietzcker, R. C., Carrara, S., de Boer, H. S., Fujimori, S., Johnson, N., Arent, D. (2017). Assessment of wind and solar power in global low-carbon energy scenarios: An introduction. Energy Economics, 64, 542551.

Appendix A: NYS Flexible Hydropower Model Objective Function

$$minimize \qquad \sum_{t \in T} NL^t \tag{10}$$

Model Constraints

All equations hold $\forall t$ unless otherwise mentioned.

Generation at each hydroelectric facility is limited to the max generation capacity at the facility. Reservoir level is similarly limited to reservoir capacity at every facility. All variables are greater than zero. For all PHES facilities, pumping and generation do not both occur in a single time step.

Net Load Constraints:

$$NL^t = D^t_{nyiso} - (P^t_{nia} + P^t_{lew} + P^t_{bg} + P^t_{sh} + P^t_{nc}) - U^t - B^t \tag{11}$$

Other Select Constraints:

$$B^t = N^t + S^t + H^t_{in,stl} \tag{12}$$

$$\frac{P^t_{nia}}{\eta_h} - \frac{P^t_{gen,lew}}{\eta_h} + \eta_h * P^t_{pump,lew} = E^{t-1}_{nia} - E^t_{nia} + H^t_{in,nia} \tag{13}$$

$$\frac{P^t_{gen,lew}}{\eta_h} - \eta_h * P^t_{pump,lew} = E^{t-1}_{lew} - E^t_{lew} \tag{14}$$

$$\frac{P^t_{gen,bg}}{\eta_h} - \eta_h * P^t_{pump,bg} = E^{t-1}_{bg} - E^t_{bg} \tag{15}$$

$$\frac{P^t_{sh}}{\eta_h} = E^{t-1}_{sh} - E^t_{sh} + H^t_{in,sh} \tag{16}$$

$$\frac{P^t_{gen,nc}}{\eta_h} - \eta_h * P^t_{pump,nc} = E^{t-1}_{nc} - E^t_{nc} \tag{17}$$

$$H^t_{sh} = \frac{1}{\tau+1} \sum_{i=t-\tau/2}^{t+\tau/2} H^i_{nyiso} - H^i_{in,nia} - H^i_{in,stl} \tag{18}$$

$$H^t_{fix} = \frac{1}{\tau+1} \sum_{i=t-\tau/2}^{t+\tau/2} H^i_{nyiso} \tag{19}$$

Appendix B: NYS Comparative Flexibility Model Objective Function

$$minimize \qquad \sum_{t \in T} \sum_{r \in R} NL^t_r \tag{20}$$

Model Constraints

All equations hold $\forall t$, $\forall r$, unless otherwise mentioned.

Generation at each hydroelectric facility is limited to the max generation capacity at the facility. Reservoir level is similarly limited to reservoir capacity at every facility. All variables are greater than zero. For the PHES facility, pumping and generation do not both occur in a single time step.

Net Load Constraints:

$$NL^t_r = D^t_{nyiso,r} + D^t_{flex,r} - H^t_{flex,r} - PS^t_{gen,r} + PS^t_{pump,r} - U^t_r - B^t_r + \sum_{r' \in R} [Z_{rr'}{}^t - (1-l_r) Z_{r'r}{}^t] \tag{21}$$

Other Select Constraints:

$$B^t_r = H^t_{fix,r} + N_r + S^t_r \tag{22}$$

$$\frac{PS^t_{gen,r}}{\eta_h} - \eta_h * PS_{pump,r} = E^{t-1}_{ps,r} - E^t_{ps,r} \tag{23}$$

$$\frac{H^t_{flex,r}}{\eta_h} = E^{t-1}_{fh,r} - E^t_{fh,r} + H^t_{in,r} \tag{24}$$

$$H^t_{in,r} = x_h * H_{tot} \tag{25}$$

$$H^t_{in,r} + H^t_{fix,r} = H_{tot,r} \tag{26}$$

$$\sum_{t=19+24m}^{7+24(m+1)} \eta_{ev} * D^t_{flex,r} = 24 * D_{ev,r}, \quad for \;\; m = 1..\frac{T}{24} \tag{27}$$

$$U^t_r \leq \sum_{n \in n_r} W^t_s \tag{28}$$

$$Z^t_{rr'} \leq L^+_{rr'} \tag{29}$$

$$Z^t_{r'r} \leq L^-_{r'r} \tag{30}$$